Applied Catalysis B: Environmental 322 (2023) 122094

Contents lists available at ScienceDirect

Applied Catalysis B: Environmental

journal homepage: www.elsevier.com/locate/apcatb

Generation of adsorbed atomic hydrogen by Pd(II) doped $Fe(OH)_2$ enables ultra-fast reductive dechlorination of trichloroethylene

Li-Zhi Huang [a,b], Yi Wang [a,b], Jia Deng [a,b,*], Jianping Yuan [a], Yitao Dai [c], Weizhao Yin [d,**]

[a] School of Civil Engineering, Wuhan University, No. 8, East Lake South Road, Wuhan, PR China
[b] School of Resources and Environmental Science, Wuhan University, Wuhan, PR China
[c] Department of Applied Chemistry, University of Science and Technology of China, Hefei 230026, PR China
[d] School of Environment, Jinan University, Guangzhou 510632, PR China

ARTICLE INFO

Keywords:
Ferrous hydroxide
Palladium
Groundwater
Ultra-fast dechlorination
Electron transfer

ABSTRACT

Trichloroethylene (TCE) is a notorious persistent pollutant in groundwater, while most reductive dechlorination processes result in the formation of toxic less-chlorinated by-products. In this work, adsorbed atomic hydrogen (H*) was produced by Pd(II) doped $Fe(OH)_2$, which was used for ultra-fast reductive dechlorination of TCE without the formation of less-chlorinated by-products. When the $Fe(OH)_2$ dosage is 0.5 mM and the Pd(II) dosage is 20 μM, TCE (42 μM) is completely removed in 60 min with the pseudo first-order reaction rate constant of 7.74 h^{-1}. Radical quenching experiment and electrochemical analysis both confirmed that adsorbed H* rather than absorbed H* contribute to the reduction of TCE. Density function theory calculation demonstrated that small Pd clusters were more beneficial to TCE dechlorination than large Pd clusters. The pseudo first-order rate constant for TCE reduction in real groundwater was as high as 0.018 min^{-1}, demonstrating the potential application of Pd/$Fe(OH)_2$ in groundwater remediation.

1. Introduction

Trichloroethylene (TCE) has been largely produced for industrial and domestic applications [1]. Inevitably, highly toxic, persistent, and poorly biodegradable TCE have been released into the environment, and TCE has been frequently detected in soil and groundwater worldwide. Reductive dechlorination can efficiently detoxify TCE, but the formation of toxic lesser-chlorinated by-products is of great concern [2,3]. The formation of toxic by-products is usually caused by the weak reduction strength of the applied reductant and the corresponding slow reductive dechlorination rates especially for dechlorinated intermediates. Reductive dechlorination of TCE to fully dechlorinated products requires the transfer of multiple electrons, and the lower the chlorinated extent of the molecules, the more difficult the reductive dechlorination occurs. As a result, lesser-chlorinated by-products accumulate along the reaction course, especially for the dechlorination process mediated by direct electron transfer [4–6]. On the other hand, atomic hydrogen (H*)-mediated indirect electron transfer shows excellent hydrodechlorination activity due to the extremely high reductive strength of H* ($E^0 = -2.106$ V) [7,8]. TCE can be reduced to ethylene (C_2H_4) and ethane (C_2H_6) under the attack of H* , and toxic persistent chlorinated intermediates are usually not formed. The reduction of H^+ to H* can be catalyzed by a variety of transition metals, of which palladium (Pd) is the most efficient one [9]. Pd-catalyzed generation of H* is a promising and highly reactive reductant for the decontamination of nitrate, nitrite, bromate, chlorate, perchlorate, N-nitrosamines and a number of chlorinated hydrocarbons (e.g., carbon tetrachloride (CT), 1,2-dichloroethane, TCE, perchloroethylene) [10]. H_2 can be activated on the surface of Pd to form H* . On the other hand, Pd can catalyze H_2O/H^+ to generate H* , thereby contributing to reductive dechlorination.

There are two types of H* species in the Pd catalyzed reaction, including H* adsorbed on Pd surface (H^*_{ads}) and H* absorbed into Pd crystal lattice (H^*_{abs}). The type of active H* species for hydrodechlorination is still under debate [11–13]. For example, H^*_{abs} has been reported to be responsible for reductive dechlorination because high H^*_{abs} solubility is related to fast reductive dechlorination rates [14]. However, the authors omit the possible presence of H^*_{ads} which may also contribute to hydrodechlorination. In contrast, electrochemical reduction of 2,4-dichlorophenol by Pd nanoparticles demonstrated that H^*_{ads} rather than H^*_{abs} was responsible for dechlorination

* Corresponding author at: School of Civil Engineering, Wuhan University, No. 8, East Lake South Road, Wuhan, PR China.
** Corresponding author.
E-mail addresses: 2019182060112@whu.edu.cn (J. Deng), weizhaoyin@jnu.edu.cn (W. Yin).

https://doi.org/10.1016/j.apcatb.2022.122094
Received 10 July 2022; Received in revised form 10 October 2022; Accepted 22 October 2022
Available online 26 October 2022

[13]. Highly reactive H^*_{ads} is readily combined to form molecular hydrogen (H_2), which unfavored hydrodechlorination [15]. Also, the hydrogen evolution can hinder the diffusion of H^+ and chlorinated organic pollutants to the surface of reductants, inhibiting the hydrodechlorination process. Similarly, our recent study showed H^*_{ads} in Ni-Fe hydroxides is more reactive than H^*_{abs} towards hydrodechlorination of TCE [15]. Thus, the types of reactive H* in Pd catalyzed hydrodechlorination and relevant mechanisms need more understanding.

The hydrolysis of Fe^{2+} at neutral or alkaline conditions in the subsurface environment can form ferrous hydroxides ($Fe(OH)_2$, white rust). $Fe(OH)_2$ is also found in the corrosion product of steel [16]. Although $Fe(OH)_2$ has reductive reactivity due to the presence of structural Fe(II), the reductive strength of $Fe(OH)_2$ is relatively low [17]. $Fe(OH)_2$ induced reductive dechlorination of TCE has been scarcely studied [18]. Fe^{2+} is an abundant, cheap and environmental-friendly electron donator in bimetallic catalyzed reductive dechlorination [19–24]. Especially in a deep groundwater environment, Fe^{2+} is abundant in the forms of ferrous minerals (e.g. white rust, green rust, magnetite and Fe^{2+}-containing clays) while electron donation by electrochemical setup is unfeasible. Thus, Fe^{2+} could be used as a promising electron donor for the Pd-catalyzed hydrodechlorination system.

In this work, we designed a $Pd/Fe(OH)_2$ system for ultra-fast TCE hydrodechlorination. The morphology and chemical composition of the $Pd/Fe(OH)_2$ is characterized. The types of active hydrogen species responsible for reductive dechlorination were identified by electrochemical analysis and radical quenching experiments. The influence of reaction parameters such as Pd content, pH, and interfering ions on the reductive dechlorination and product distribution were studied.

2. Materials and methods

2.1. Chemicals and experimental setup

Detailed information on chemicals used in this work is shown in Text S1. $Fe(OH)_2$ was synthesized using a precipitation method. NaOH solution was slowly added into $FeCl_2$ solution under stirring until the pH was 8.2 (Fig. S1). The formed $Fe(OH)_2$ suspensions were stirred magnetically for 2 h, and stood still for 12 h. Fig. S2 shows the schematic illustration for the synthesis of $Fe(OH)_2$. The prepared $Fe(OH)_2$ suspensions and $PdCl_2$ solution were added into 10 mL reaction glass vials, and the final volume of the mixed solution was adjusted to 5 mL using oxygen-free ultrapure water. Subsequently, TCE saturated aqueous solution was added into the reaction vials and capped immediately. The above operations were carried out in an anoxic glovebox containing 99.9% argon. The sealed vials were taken out from the anoxic glovebox and placed at a rotary agitator for reaction (40 rpm). The influence of reaction parameters on dechlorination was studied and the experimental details are shown in Text S1. Parameters of the real groundwater matrix used in this work can be found in our previous study [15].

2.2. Analytical methods

The concentration of Fe^{2+} was determined using *1,10*-phenanthroline regents [15]. The concentration of TCE and its degradation products were analyzed by a gas chromatograph according to our previous study [15]. TCE removal rate was calculated using pseudo-first-order kinetics (Eq. 1). C and C_0 represent TCE concentration and TCE initial TCE concentration. k represents pseudo first-order reaction rate constant. t represents reaction time.

$$-\ln(C/C_0) = k \times t \quad (1)$$

2.3. Material characterization

The particles formed before and after the reaction were collected and air-dried in an anoxic glovebox for characterization. The crystalline structure of $Pd/Fe(OH)_2$ was analyzed by X-ray diffraction (XRD, X'Pert PRO, PANalytical, Netherlands). The valence states of Fe and Pd in $Pd/Fe(OH)_2$ were analyzed by X-ray photoelectron spectroscopy (XPS, ESCALAB250Xi, Thermo Fisher Scientific, USA). The morphology of $Pd/Fe(OH)_2$ was determined by transmission electron microscopy (TEM) (JEM-2100, JEOL, Japan) equipping energy dispersive X-ray spectroscopy (EDX). An electrochemical workstation (CHI 630, CH Instruments, China) was used to identify the types of H* , the interfacial electron transfer and the corrosion properties of $Pd/Fe(OH)_2$. Fourier transform infrared (FTIR, FTIR5700, Thermo, USA) spectra was obtained and analyzed to determine the functional groups of $Pd/Fe(OH)_2$.

2.4. DFT calculation

The conformation of $Fe(OH)_2$ and $Pd/Fe(OH)_2$ was optimized based on B3LYP [25,26] density functional theory (DFT) using Gaussian 09 package (Revision B.01) [27]. More detailed information on DFT calculation can be found in our previous study [15].

3. Results and discussions

3.1. TCE dechlorination by $Pd/Fe(OH)_2$

TCE cannot be removed in the presence of $Fe(OH)_2$ or $PdCl_2$ alone (Fig. S3a-b). Under acidic conditions, TCE removal was negligible in a solution containing Fe^{2+} and $PdCl_2$, indicating the electrons of Fe^{2+} ions were not transferred to TCE for dechlorination (Fig. S3c). The bimetallic system containing $PdCl_2$ and nZVI (Pd/nZVI) can dechlorinate TCE, which transformed 42 μM of TCE to 27.2% ethylene (C_2H_4) and 19.0% ethane (C_2H_6) after 120 min (Fig. S3d). Surprisingly, the novel bimetallic system consisting of $PdCl_2$ and $Fe(OH)_2$ ($Pd/Fe(OH)_2$) had a higher TCE removal efficiency than Pd/nZVI system (Fig. 1a). The pseudo-first-order rate constant of TCE removal by $Pd/Fe(OH)_2$ was 0.129 min^{-1}, which was higher than 0.056 min^{-1} of nZVI/Pd (Fig. S4). In order to determine the dechlorination path of TCE, the products distribution of TCE with different initial TCE concentrations were monitored in $Pd/Fe(OH)_2$ system during 120 min of reaction (Fig. S5). The main dechlorination products of TCE were C_2H_4 and C_2H_6, and toxic lesser-chlorinated products were not formed. More C_2H_6 was produced compared with C_2H_4 when the initial TCE concentration was lower than 42 μM, indicating the hydrogenation of ethylene was dominant in $Pd/Fe(OH)_2$ system (Fig. 1b). In contrast, more amount of C_2H_4 was produced compared with C_2H_6 when TCE initial concentration was higher than 42 μM. When TCE concentration was 42 μM, the production of C_2H_4 and C_2H_6 were 17.1% and 33.5%, respectively. The total complete dechlorinated products in $Pd/Fe(OH)_2$ system was more than that in Pd/nZVI system, which reflected the high dechlorination reactivity of $Pd/Fe(OH)_2$ system.

Fig. 1c showed the strong diffraction peak of $Fe(OH)_2$ (100) at 30.6∘ (JCPDS card No 13–0089) before reaction. The particles after reaction show a broad diffraction peak at 21.5∘, which may correspond to other poorly-crystalized ferric (oxy)hydroxides. The Pd 3d XPS showed the peaks at 335.1 eV and 340.4 eV corresponding to Pd(0), and the peaks at 336.0 eV and 341.3 eV were belonged to Pd(II) (Fig. 1d) [28]. The peaks at 710.4 and 723.9 eV of Fe 2p belonged to Fe(II), and peaks at 712.5 and 726.1 eV belonged to Fe(III), respectively (Fig. 1e) [29]. The presence of Fe(III) and Pd(0) confirmed the redox reaction between Fe(II) and Pd(II). In addition, the mass loss during TCE dechlorination could be resulted from the adsorption of TCE by Pd(0) which was obvious at a low ratio of TCE/Pd. The Pd surface prefers to break the π bond of C═C and form the C–Pd σ bonds [30]. This adsorbed TCE is not further reduced, which may be due to the inhibitory effect of C–Pd σ bonds on the

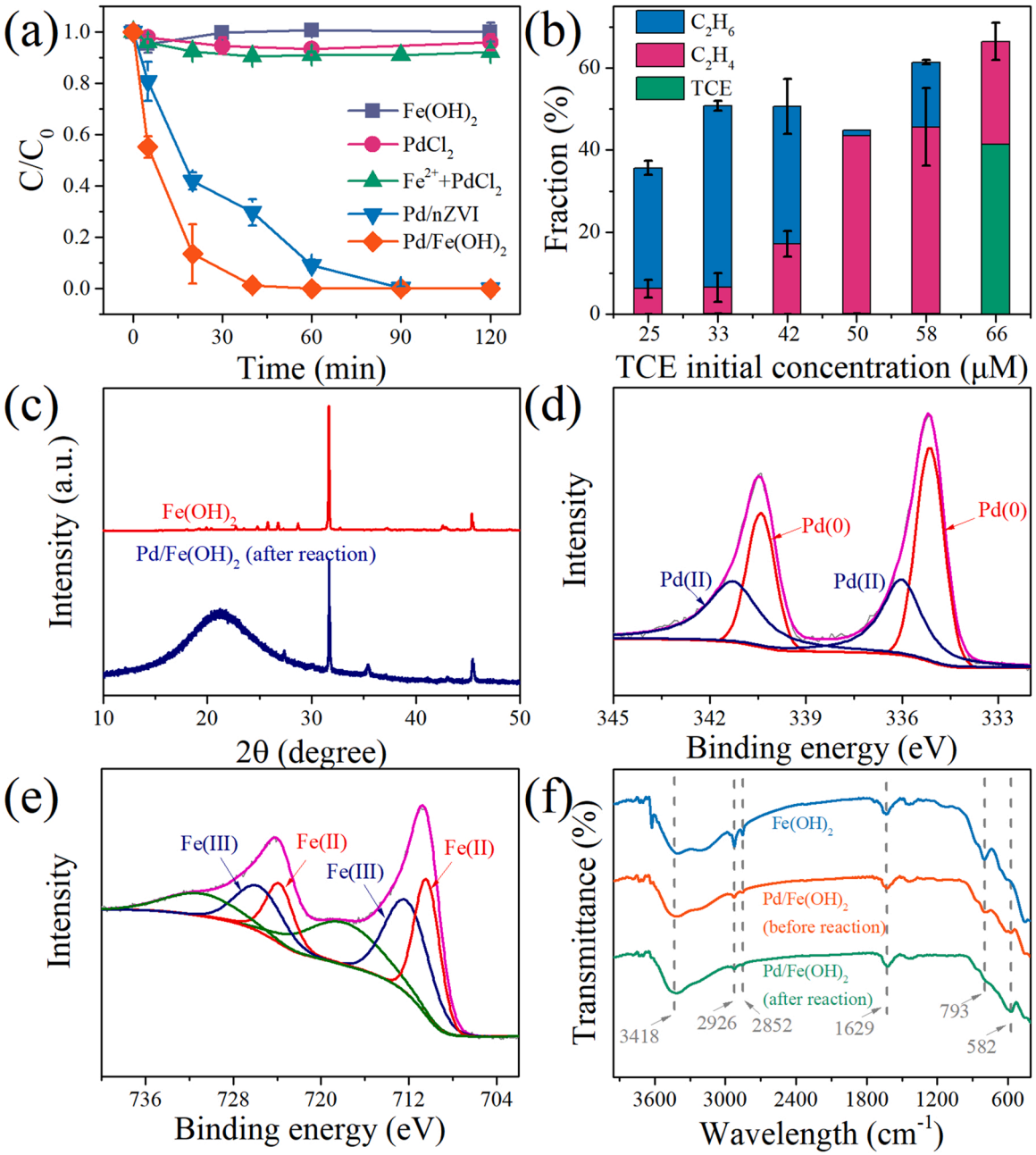

Fig. 1. (a) TCE removal by $Fe(OH)_2$, $PdCl_2$, Fe^{2+}+$PdCl_2$ (pH < 3.0), Pd/nZVI and $Pd/Fe(OH)_2$. (b) Fraction of dechlorinated products with different initial TCE concentrations in $Pd/Fe(OH)_2$ system. Experimental conditions: Fe(II) = 0.5 mM, Pd = 20 μM, TCE = 42 μM, pH = 7.5. (c) XRD patterns of $Fe(OH)_2$ and $Pd/Fe(OH)_2$ after reaction. XPS spectra of (d) Pd 3d and (e) Fe 2p in $Pd/Fe(OH)_2$. (f) FTIR of $Fe(OH)_2$ and $Pd/Fe(OH)_2$.

electron transfer between Pd and Fe(II). Fig. 1f shows the FTIR spectra of the as-synthesized $Fe(OH)_2$ and $Pd/Fe(OH)_2$. The bands at 3405 and 793 cm^{-1} could be assigned to the O–H vibration of $Fe(OH)_2$ and Fe–O bonds [31,32]. The bands at 2926 and 2852 cm^{-1} was attributed to H_2O–anions bridging mode. The band at 1629 cm^{-1} was belong to vibration of adsorbed water between layer hydroxides [33]. The band at 582 cm^{-1} was assigned to Pd–O bond [34]. When Pd(II) was introduced into $Fe(OH)_2$ suspensions, the structure of hydroxides was not changed. Pd cannot be oxidized under oxygen-free conditions, thus the formation of Pd–O bond was attributed to the olation effect. After hydroxylation, electron transferred from $Fe(OH)_2$ to Pd(II) causing the formation of Pd (0).

SEM image showed $Fe(OH)_2$ consists of multi-layers irregularly shaped flakes (Fig. S6a), which is also shown by TEM image (Fig. S6b). After the dechlorination reaction, the edge of $Pd/Fe(OH)_2$ particles became sharp (Fig. 2a). $Pd/Fe(OH)_2$ particles still show multi-layers irregularly shaped flakes (Fig. 2b), and typical hexagonal morphology of Fe(II)-Fe(III) hydroxides was found in the TEM images (Fig. 2c). This phenomenon indicates a possible formation of other (oxy)hydroxides via the oxidation of $Fe(OH)_2$ [22]. In these hexagonal particles, lattice spacing of 2.2 Å corresponding the (111) plane of Pd (JCPDS card No 65–2867) was observed (Fig. 2d). The diffraction peak of Pd (111) lattice plane was not showed in XRD pattern due to the extremely low Pd/Fe dosage ratio. EDX of $Pd/Fe(OH)_2$ particles also showed the extremely low Pd content (Fig. S7). However, the clear lattice spacing in TEM and XPS data both confirmed the presence of Pd(0). According to the elemental mapping images (Fig. 2e), Fe, O and Pd was evenly distributed on the surface of $Pd/Fe(OH)_2$ particles [35]. This result demonstrated that Pd(II) binding site was evenly distributed on the surface of $Fe(OH)_2$.

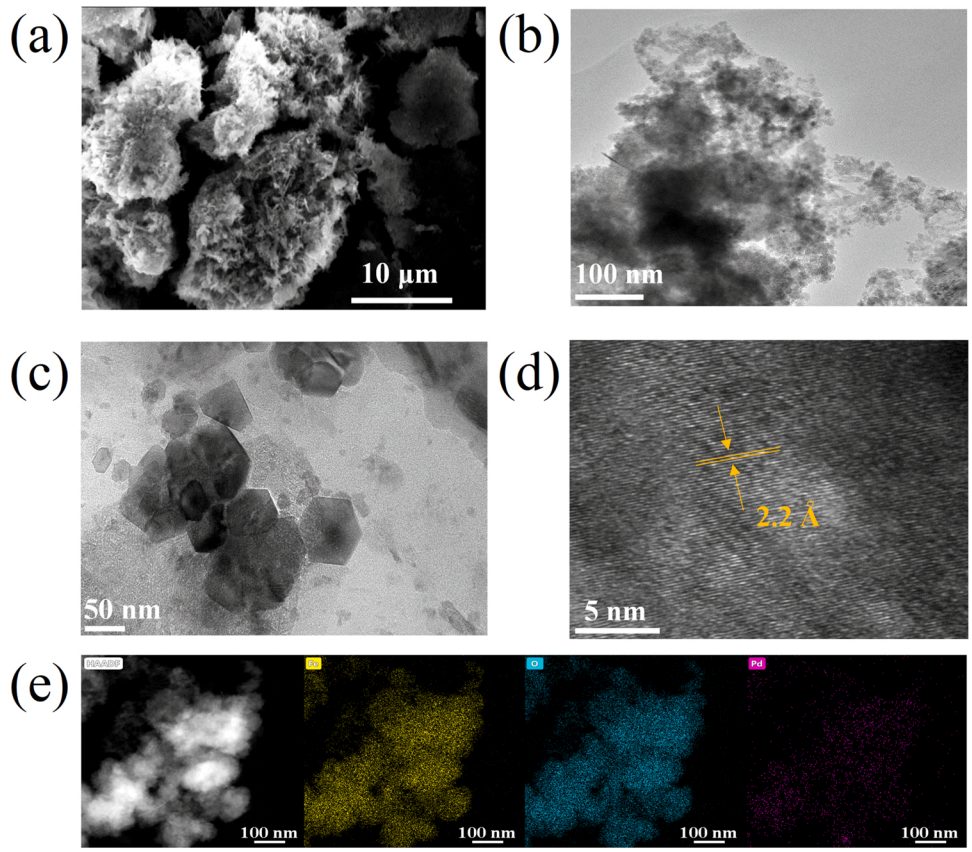

Fig. 2. (a) SEM and (b) TEM image of formed Pd/Fe(OH)$_2$ particles after reaction. (c-d) HRTEM image of formed Pd/Fe(OH)$_2$ particles after reaction. (e) Elemental mapping of Pd/Fe(OH)$_2$ particles.

3.2. *Effect of H* on dechlorination*

Atomic hydrogen (H*) can be efficiently generated for dechlorination in Pd catalyzed reduction system [36]. In order to identify the active species on TCE dechlorination, TBA as H* quencher was introduced into Pd/Fe(OH)$_2$ system. The presence of 200 mM TBA significantly decreased the removal efficiency of TCE, which was only 62.7% after 120 min reaction (Fig. 3a). Also, the generation of dechlorinated products decreased from 50.6% (17.1% C_2H_4 and 33.5% C_2H_6) to 27.0% (27.0% C_2H_4 and 0% C_2H_6). The inhibitory effect of TCE dechlorination in the presence of 200 mM and 1 M TBA was similar (Fig. 3b). The presence of excess concentration TBA did not affect the transformation of the remaining 27.0% of TCE to C_2H_4, indicating that the dechlorination of TCE was not only resulted from the contribution of H* , but also the direct electron transfer on Pd(0) active sites. In order to exclude the solvation effect of TBA, NO_3^- was also selected as the H* quencher because NO_3^- can be reduced by H* to NO_2^- and NH_4^+ [1]. The removal efficiency of TCE was 63.2% and the generation of C_2H_4 was only 9.4% in the presence of 200 mM NO_3^- (Fig. 3c). As the concentration of NO_3^- was further increased to 1 M, TCE dechlorination was almost completely inhibited (Fig. 3d). Notably, the mass loss was also decreased in the presence of 1 M NO_3^-. The excess NO_3^- can not only react with H* , but also directly accept electrons from Fe(OH)$_2$ [37]. The competition for electrons between NO_3^- and Pd(II) unfavored the reduction of Pd(II) to Pd(0), thereby inhibiting the adsorption of TCE on Pd(0) surface. Fig. 3e showed the cyclic voltammetry (CVs) of the formed particles in Pd/Fe(OH)$_2$ system. Three oxidation peaks at − 0.8 V, − 0.2 V and 0 V (vs. Ag/AgCl) could be assigned to the oxidation of H_2, H_{abs}* and H_{ads}* , respectively. When TCE was added into the electrolyte, the oxidation peak of H_{ads}* disappeared. Therefore, the H_{ads}* generated on the Pd(0) surface is responsible for TCE reduction, while H_{abs}* was inert for dechlorination [13,29]. He etc. also found H_{ads}* rather than H_{abs}* is responsible for TCE dechlorination by Pd/nZVI system [29]. It is likely that TCE molecules are difficult to diffuse into the Pd crystal lattice where H_{ads}* is located. On the other hand, TCE molecules can diffuse on the surface of Pd where H_{ads}* and TCE react.

3.3. *Effect of Pd dosage and pH*

Pd(0) as electronic conductor catalyzed H^+/H_2O to generate H* , which led to the reductive dechlorination of TCE. In order to investigate the role of Pd, TCE reduction in Pd/Fe(OH)$_2$ systems with different Pd concentrations was conducted. The pseudo first-order rate constants increased with Pd dosage from 5 μM to 25 μM and then slightly decreased at 30 μM (Fig. 4a). At 5 μM Pd dosage, the dechlorination efficiency of TCE was low due to the insufficient amount of Pd(0) catalytic sites in the Pd/Fe(OH)$_2$ system (Fig. 4b). When Pd dosage increased to 10 μM, C_2H_4 was the main dechlorinated products of TCE. When Pd dosage increased to 20 μM, C_2H_6 became the dominant product (Fig. S8). The transformation from C_2H_4 to C_2H_6 needs a high amount of H* , which can be produced with high Pd dosage (> 20 μM). These phenomena demonstrate that a relatively high amount of Pd is essential to generate sufficient reactive H* .

The interfacial electron transfer of Pd/Fe(OH)$_2$ with various Pd contents was further investigated. The arc radius was decreased with increasing Pd dosage from 5 μM to 25 μM (Fig. 5a), which corresponded to the increase of interfacial charge transfer rate [38]. Compared with 25 μM Pd dosage, Pd dosage at 30 μM had a larger arc radius reflecting a slower interfacial charge transfer rate. These results were consistent with the slightly decreased TCE removal efficiency for Pd dosage at 30 μM compared with that at 25 μM (Fig. 4a). The corrosion currents of Pd/Fe(OH)$_2$ particles can be obtained by fitting the Tafel curves (Fig. S9,

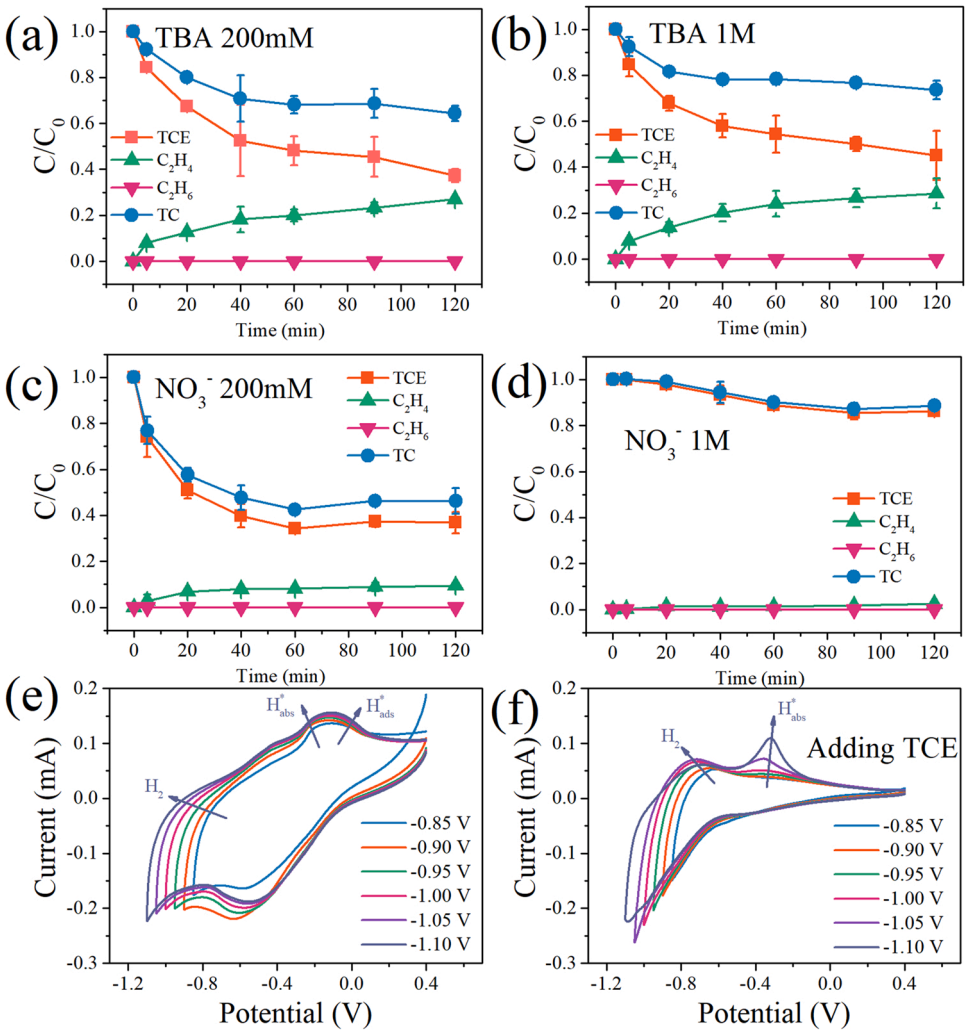

Fig. 3. TCE dechlorination in $Pd/Fe(OH)_2$ system in the presence of (a) 200 mM TBA, (b) 1 M TBA, (c) 200 mM NO_3^- and (d) 1 M NO_3^-. (TC represents total carbon balance.) Experimental conditions: Fe(II) = 0.5 mM, Pd = 20 μM, TCE = 42 μM, pH = 7.5. (e) CVs of $Pd/Fe(OH)_2$ in Ar-saturated 50 mM Na_2SO_4 solution (e) without TCE and (f) with 0.4 mM TCE (starting potential of 0.40 V, scanning rate of 50 mV s^{-1}).

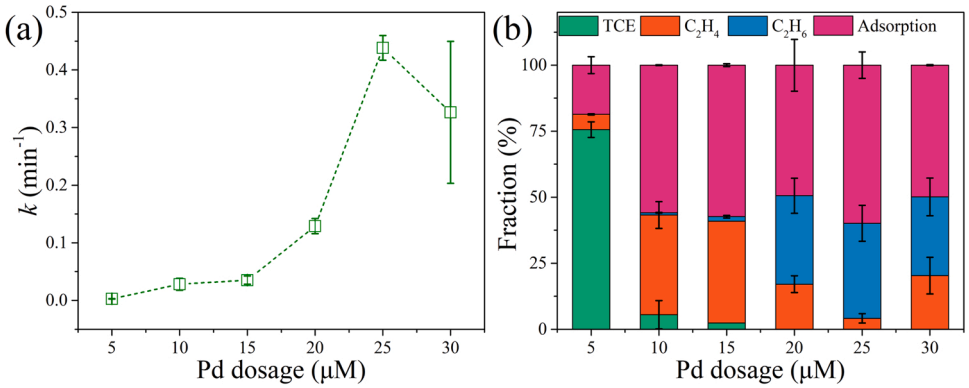

Fig. 4. Effect of Pd dosage on (a) pseudo first-order reaction rates of TCE reduction, (b) products distribution after 120 min reaction in $Pd/Fe(OH)_2$ systems. Experimental conditions: Fe(II) = 0.5 mM, TCE = 42 μM, pH = 7.5.

Fig. 5b). The corrosion current of $Pd/Fe(OH)_2$ particles maintained a relatively high value for Pd dosage ranging from 10 to 25 μM. However, $Pd/Fe(OH)_2$ particles with 30 μM of Pd dosage had the lowest corrosion current. Pd as electron-acceptor in $Pd/Fe(OH)_2$ system was reduced to Pd(0) by $Fe(OH)_2$. Pd with high dosage can compete electrons with TCE in $Pd/Fe(OH)_2$ system. Therefore, the decreased electron transfer rates with high Pd dosage led to a slightly decreased TCE dechlorination rate and a suppressed transformation of C_2H_4 to C_2H_6.

Since H* is produced via the catalytic reduction of H^+, TCE reduction in $Pd/Fe(OH)_2$ systems at different pHs were tested. The TCE dechlorination rates increased from pH 5.5 to pH 8.5 and decreased from pH 8.5 to pH 11.5 (Fig. 6a). At pH 5.5 and pH 6.5, $Fe(OH)_2$ particles were

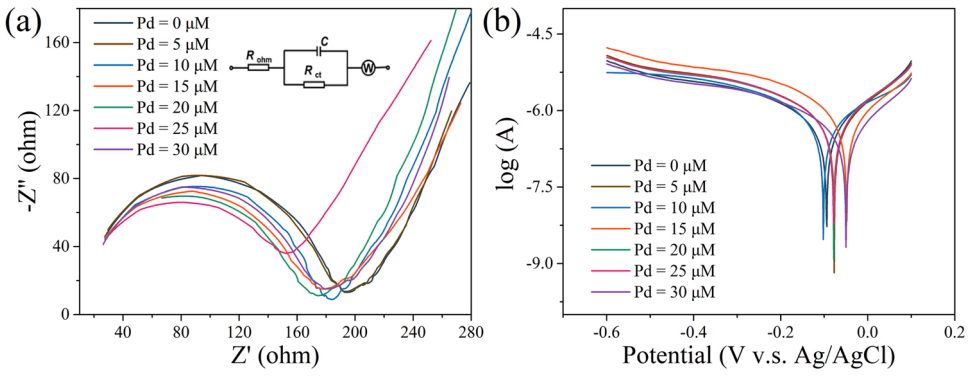

Fig. 5. (a) The Nyquist plots of Pd/Fe(OH)$_2$ with different Pd dosages. Insert image is equivalent circuit diagrams. (b) Tafel scans of Pd/Fe(OH)$_2$ with different Pd dosages.

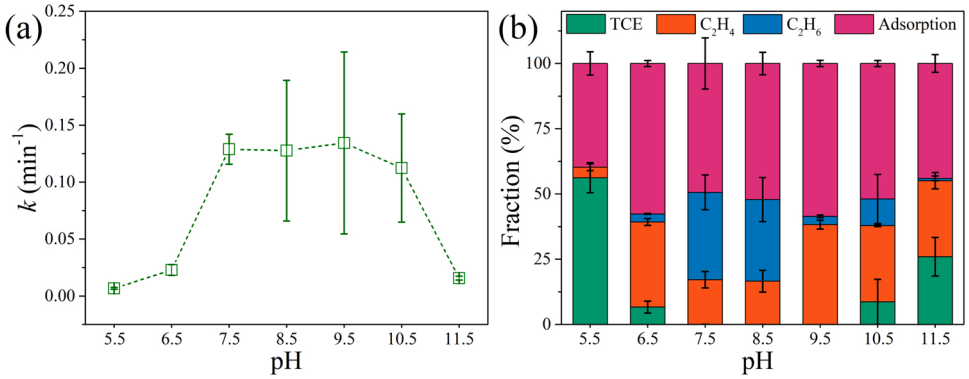

Fig. 6. Effect of pH on (a) pseudo first-order reaction rates of TCE reduction, (b) products distribution after 120 min reaction in Pd/Fe(OH)$_2$ systems. Experimental conditions: Fe(II) = 0.5 mM, Pd = 20 μM, TCE = 42 μM.

dissolved. The dissolved Fe(II) cannot efficiently reduce Pd(II) to Pd(0), thereby inhibiting the reduction of TCE. Therefore, TCE cannot be completely removed in Pd/Fe(OH)$_2$ systems after 120 min at pH 5.5 and pH 6.5 (Fig. 6b). TCE dechlorination rates and product distribution were similar at pH 7.5 and pH 8.5 (Fig. S10). The dominant dechlorination product was C_2H_4 at pH 9.5, indicating less amount of H* was produced at slightly alkaline conditions. Due to the low concentration of H^+ at pH 10.5 and 11.5, the TCE dechlorination and C_2H_4-to-C_2H_6 conversion were further inhibited.

3.4. Mechanism of TCE dechlorination

The layer structure of Fe(OH)$_2$ was built via DFT (Fig. S11). The cluster of three Fe(OH)$_2$ molecules was built to simulate the electron transfer between Fe(OH)$_2$ and Pd(II). According to a previous publication, the spin was selected as 13-et [39]. One Pd(II) atom was located around the optimized Fe(OH)$_2$ cluster and the complex conformation was optimized. There were two binding sites of Pd(II) in Fe(OH)$_2$ cluster including O and Fe(II) (Fig. 7a). For O binding sites, Pd(II) complexed with hydroxyl groups of Fe(OH)$_2$ and the Fe−O bond-length was 2.2 Å. After complexation, the atomic charge of Pd decreased from 2.000 to

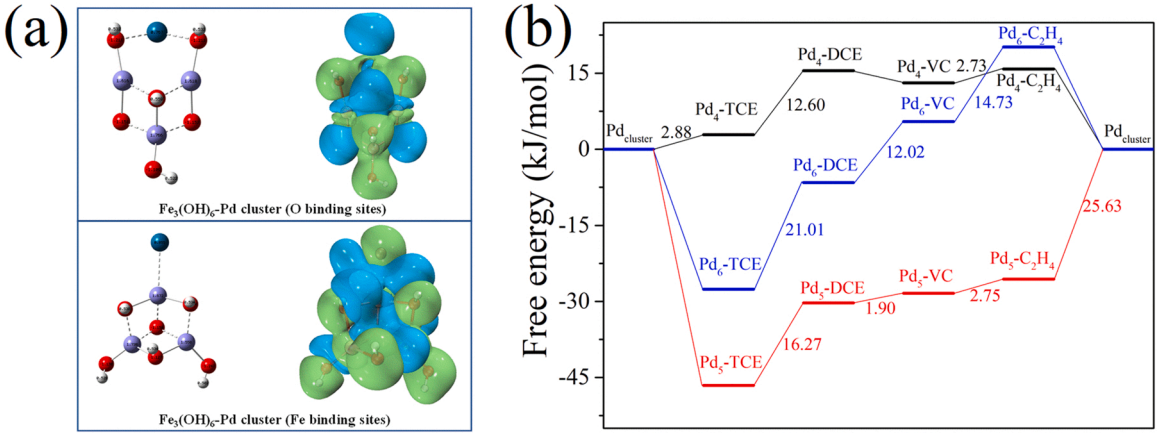

Fig. 7. The geometries with NBO atomic charge and charge difference of $Fe_3(OH)_6$-Pd cluster. The isosurface is set as 0.01. (b) The free energy change of TCE dechlorination on Pd clusters.

0.767. The calculated binding energy of the $Fe(OH)_2$ cluster and Pd(II) was −554.76 kJ/mol. For Fe binding sites, Fe−Pd bond-length was 2.8 Å and the atomic charge of Pd decreased from 2.000 to 0.855 after complexation. The binding energy of the $Fe(OH)_2$ cluster and Pd(II) was −437.67 kJ/mol. The calculated binding energy was −437.67 kJ/mol. Therefore, O binding sites transfer electron from $Fe(OH)_2$ to Pd(II), which was thermodynamically favorable. In the charge difference image (Fig. 7a), the blue isosurface area around Pd located in O binding sites, while green isosurface area around Pd loated in Fe binding sites. Green and blue correspond to the isopleths of density difference= 0.01 and − 0.01 respectively, representing the main areas where the electron density increases and decreases. Thus, Fe binding sites may be more conducive to transfer electrons from reductive Pd to H^+/H_2O or TCE molecules.

Due to extremely low Pd dosage, Pd diffraction peak was not observed in XRD patterns of $Pd/Fe(OH)_2$ particles. In addition, XPS data shows the presence of Pd(0) and Pd was evenly distributed in $Pd/Fe(OH)_2$ particles. Thus, we speculated that Pd (0) is distributed on the $Pd/Fe(OH)_2$ particle surface in the form of polyatomic clusters. Subsequently, the geometries of the polyatomic Pd(0) clusters (Pd_4, Pd_5 and Pd_6) with various spin states were optimized (Fig. S12) [40]. Also, the geometries and spin density of Pd cluster-TCE, Pd cluster-DCE, Pd cluster-VC and Pd cluster-C_2H_4 complexes were optimized. Finally, the calculated energy barriers of dechlorination can be obtained in Fig. 7b. Pd_5 and Pd_6 clusters were beneficial to TCE adsorption. The highest dechlorination energy barriers for Pd_4, Pd_5 and Pd_6 were 12.60, 16.27 and 21.01 kJ/mol, respectively. This result demonstrated that a small Pd cluster was more beneficial to TCE dechlorination than a large Pd cluster. This may explain the decreased dechlorination rate when the Pd dosage increase from 25 μM to 30 μM, since a high Pd dosage at 30 μM may lead to the formation of a relatively large Pd cluster. Notably, 25.63 kJ/mol is needed for the desorption of C_2H_4 molecule from the Pd_5 cluster, which was higher than the dechlorination energy barriers. This result was attributed to the strong binding energy in Pd_5-C_2H_4 due to the incompletely symmetrical structure of the Pd_5 cluster. This result can also explain the mass loss during the dechlorination of TCE by $Pd/Fe(OH)_2$, which is resulted from the formation of the C–Pd σ bonds.

The mechanism of TCE dechlorination is illustrated in Fig. 8. When $PdCl_2$ was mixed with $Fe(OH)_2$, Pd(II) was reduced to Pd(0) by $Fe(OH)_2$ on O and Fe binding sites [41,42]. Multiple Pd(0) atoms can form Pd(0) clusters which provide the active sites for TCE dechlorination. TCE was adsorbed on the surface of Pd(0) due to the formation of the C–Pd σ bonds. Pd(0) catalyzed the reduction of H_2O/H^+ to form H*, which reduced TCE to ethylene and ethane. In addition, TCE also can be dechlorinated via directly electron transfer on Pd(0) surface. As a result, parts of $Fe(OH)_2$ were oxidized to ferric (oxy)hydroxides which show a hexagonal morphology.

3.5. Application

The real groundwater may contain various anions such as CO_3^{2-}, SO_4^{2-}, PO_4^{3-} and SiO_3^{2-}. In addition, natural organic matters such as humic acid (HA) may affect reductive dechlorination. Thus, effect of background anions and HA on TCE dechlorination by $Pd/Fe(OH)_2$ was studied. The presence of CO_3^{2-} and SO_4^{2-} show very limited influence on TCE removal (Fig. 9a). The presence of PO_4^{3-} and SiO_3^{2-} inhibited the removal of TCE due to the complexation between PO_4^{3-} or SiO_3^{2-} with Fe $(OH)_2$ (Fig. 9b, Fig. S13). HA slightly inhibit the reduction of TCE, because HA as an electron acceptor may compete with TCE for electrons in $Pd/Fe(OH)_2$ system. The potential application of $Pd/Fe(OH)_2$ system in groundwater remediation was further investigated by carrying out the reaction in real groundwater. Around 87.8% of TCE was removed by $Pd/Fe(OH)_2$ in real groundwater matrices and 30.6% of ethylene was generated (Fig. 9c). The pseudo first-order rate constant of TCE removal by $Pd/Fe(OH)_2$ in real groundwater was as high as 0.018 min^{-1}, which showed the high reduction ability of $Pd/Fe(OH)_2$ system (Fig. S14).

The reusability of $Pd/Fe(OH)_2$ was investigated for TCE removal for four cycles. In every cycle experiment, $Fe(OH)_2$ as electron donor was freshly added into the system. TCE almost can be completely removed after 60 min (Fig. 10a). Furthermore, the production of complete dechlorinated products in second, third and fourth cycle were 38.6%, 38.4% and 37.4%, respectively (Fig. 10b). C_2H_6 content was higher than C_2H_4 content in the cycle experiments, which was attributed to the abundant H* generated by the formed Pd(0) active sites. The high reusability of $Pd/Fe(OH)_2$ confirms the high catalytic stability of Pd(0) during the TCE dechlorination reaction.

The reduction rates of TCE by various Pd-Fe systems are summarized in Table S1. The $Pd/Fe(OH)_2$ system developed in this work shows one of the highest dechlorination reactivities compared with the other reported Pd-Fe systems. It should be noted that most previous reported Pd-Fe systems were developed via a borohydride-reduction approach, and the high toxicity and high cost of borohydride may impede their practical applications. Also, nZVI is relatively expensive and readily for aggregation. In contrast, the cheap and environment-abundant Fe(II) (exist as $Fe(OH)_2$ at near-neutral pHs) was used as an efficient electron donor for both Pd(0) generation and subsequent hydrodechlorination of TCE in this work. Iron is abundant in the subsurface environment, of which $\sim 3.5 \times 10^{12}$ mol/year is involved in the geochemical Fe(II)/Fe(III) redox cycle [43]. These environment-abundant Fe(II) could be used in-situ as an electron pool for reductive dechlorination in future

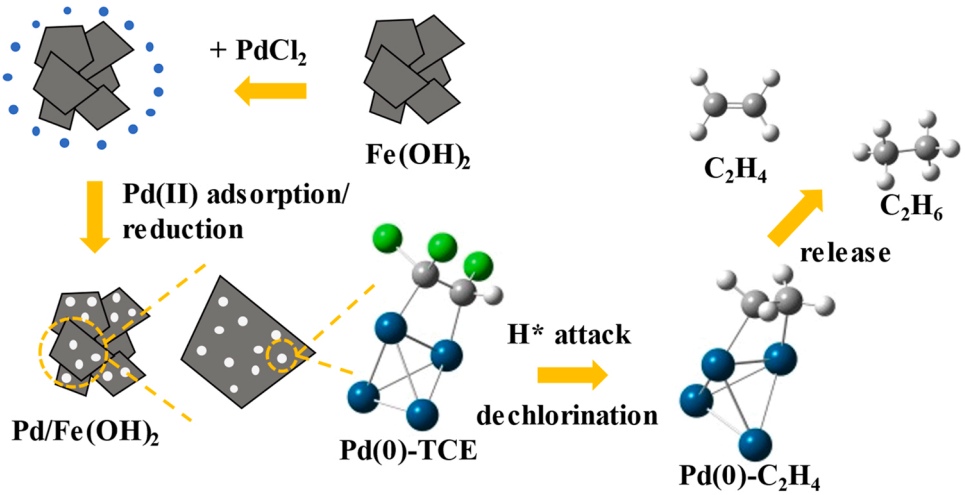

Fig. 8. The mechanism of TCE dechlorination in $Pd/Fe(OH)_2$ system.

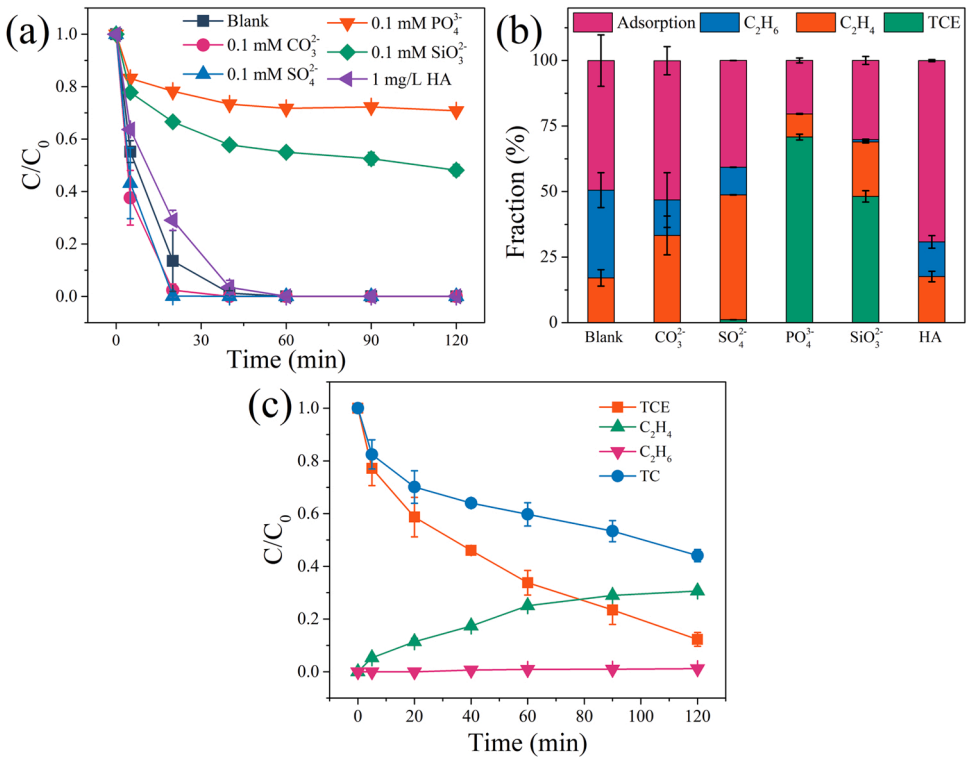

Fig. 9. (a) TCE removal in Pd/Fe(OH)$_2$ system in the presence of CO_3^{2-}, SO_4^{2-}, PO_4^{3-}, SiO_3^{2-} and humic acid. (b) products distribution after 120 min reaction in Pd/Fe(OH)$_2$ system. Experimental conditions: Fe(II) = 0.5 mM, Pd = 20 μM, TCE = 42 μM, pH = 7.5. (c) TCE reduction by Pd/Fe(OH)$_2$ in real oxygen-free groundwater. (TC represents total carbon balance.) Experimental conditions: Fe(II) = 2.0 mM, Pd = 80 μM, TCE = 42 μM, pH = 7.5.

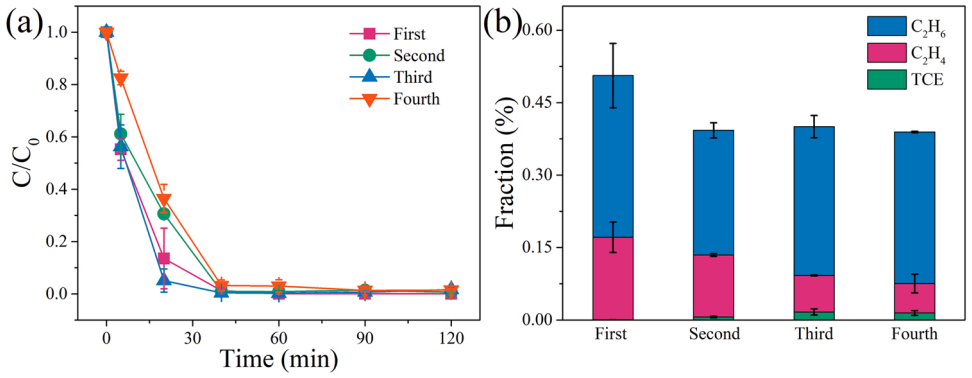

Fig. 10. (a) The reusability of Pd/Fe(OH)$_2$ and (b) the corresponding fraction of products. Experimental conditions: Fe(II) = 2.0 mM, Pd = 80 μM, TCE = 42 μM, pH = 7.5.

applications. Pd(II) aqueous solution could be injected into Fe(II)-rich groundwater environment for in situ synthesis of Pd/Fe(OH)$_2$. The volume of the injected Pd(II) aqueous solution is relatively small due to its high reactivity, which is also favourable for easy injection. However, the high cost of Pd may hinder the large-scale application of the developed Pd/Fe(OH)$_2$ system. Future work should focus on the reactivity regeneration of the deactivated Pd/Fe(OH)$_2$ particles to reduce the cost in practical applications, which may be realized by replenishing the Fe(II) electron pool via possible iron-reducing microorganisms [44].

4. Conclusion

In this work, Fe(OH)$_2$ was doped with Pd(II) which led to the generation of adsorbed H* for ultra-fast reductive dechlorination of TCE. TCE was fully dechlorinated to C_2H_4 and C_2H_6 by Pd/Fe(OH)$_2$ without the formation of less-chlorinated by-products. Pd(II) was reduced to Pd (0) by Fe(OH)$_2$, and Pd(0) is responsible for the H* generation with Fe(OH)$_2$ as an electron donor. Radical quenching experiment and electrochemical analysis both confirmed that adsorbed H* rather than absorbed H* is responsible for the ultra-fast hydrodechlorination of TCE. The Pd dosage at 25 μM resulted in the highest reduction rate of TCE, which could stem from the highest interfacial electron transfer rates and the most negative corrosion potential at 25 μM Pd dosage. Fe and Pd particles were dissolved at acidic conditions and the concentration of proton was low at alkaline conditions. Thus, the reductive dechlorination rate is the highest at the near-neutral pH conditions, at which the generation of H* is favoured. The presence of PO_4^{3-} and SiO_3^{2-} inhibited the TCE reduction, while the inhibition effect of CO_3^{2-}, SO_4^{2-} and HA on TCE reduction is negligible. Pd/Fe(OH)$_2$ system showed excellent TCE reduction efficiency comparing with previously reported reductive systems. Low cost and easy-to-prepared Fe(OH)$_2$ is a promising reductant that can be considered as a potential replacement of nZVI

in the remediation of TCE-contaminated groundwater.

CRediT authorship contribution statement

Li-Zhi Huang: Conceptualization, Investigation, Visualization, Writing – original draft. **Yi Wang**: Investigation, Writing. **Jia Deng**: Investigation, Visualization, Writing. **Jianping Yuan**: Investigation, Writing. **Yitao Dai**: Investigation, Writing. **Weizhao Yin**: Conceptualization, Investigation, Writing.

Declaration of Competing Interest

The authors declare that they have no known competing financial interests or personal relationships that could have appeared to influence the work reported in this paper.

Data Availability

No data was used for the research described in the article.

Acknowledgements

This work was financially supported by the National Natural Science Foundation of China (Grant No. 51978537, 52270165 and 41807188), the Fundamental Research Funds for the Central Universities (2042021kf0201), Guangzhou Science Technology and Innovation Commission (202102020345), and the Natural Science Foundation of Guangdong Province (2021A1515011622). The numerical calculations in this paper have been done on the supercomputing system in the Supercomputing Center of University of Science and Technology of China. We thank the Core Facility of Wuhan University for XPS analysis.

Appendix A. Supporting information

Supplementary data associated with this article can be found in the online version at doi:10.1016/j.apcatb.2022.122094.

References

[1] J. Deng, F. Wu, S. Gao, D.D. Dionysiou, L.-Z. Huang, Self-activated $Ni(OH)_2$ cathode for complete electrochemical reduction of trichloroethylene to ethane in low-conductivity groundwater, Appl. Catal. B Environ. 309 (2022), 121258.
[2] Y.S. Han, S.P. Hyun, H.Y. Jeong, K.F. Hayes, Kinetic study of *cis*-dichloroethylene (*cis*-DCE) and vinyl chloride (VC) dechlorination using green rusts formed under varying conditions, Water Res. 46 (19) (2012) 6339–6350.
[3] X.M. Yang, C. Zhang, F. Liu, J. Tang, Groundwater geochemical constituents controlling the reductive dechlorination of TCE by nZVI: Evidence from diverse anaerobic corrosion mechanisms of nZVI, Chemosphere 262 (2021), 127707.
[4] J. Ai, H. Ma, D.J. Tobler, M.C. Mangayayam, C. Lu, F.W.J. van den Berg, W. Yin, H. C. Bruun Hansen, Bone char mediated dechlorination of trichloroethylene by green rust, Environ. Sci. Technol. 54 (6) (2020) 3643–3652.
[5] J. Ai, W. Yin, H.C.B. Hansen, Fast dechlorination of chlorinated ethylenes by green rust in the presence of bone char, Environ. Sci. Technol. Lett. 6 (3) (2019) 191–196.
[6] Y. Li, M. Cai, B. Ji, F. Wu, L.-Z. Huang, Pyridinic nitrogen enables dechlorination of trichloroethylene to acetylene by green rust: performance, mechanism and applications, Sci. Total Environ. 824 (2022), 153825.
[7] B. Liu, H. Zhang, Q. Lu, G. Li, F. Zhang, A Cu-Ni bimetallic cathode with nanostructured copper array for enhanced hydrodechlorination of trichloroethylene (TCE), Sci. Total Environ. 635 (2018) 1417–1425.
[8] R. Mao, C. Huang, X. Zhao, M. Ma, J. Qu, Dechlorination of triclosan by enhanced atomic hydrogen-mediated electrochemical reduction: Kinetics, mechanism, and toxicity assessment, Appl. Catal. B Environ. 241 (2019) 120–129.
[9] R. Mao, H. Lan, L. Yan, X. Zhao, H. Liu, J. Qu, Enhanced indirect atomic H* reduction at a hybrid Pd/graphene cathode for electrochemical dechlorination under low negative potentials, Environ. Sci. Nano 5 (10) (2018) 2282–2292.
[10] B.P. Chaplin, M. Reinhard, W.F. Schneider, C. Schüth, C.J. Werth, Critical review of Pd-based catalytic treatment of priority contaminants in water, Environ. Sci. Technol. 46 (7) (2012) 3655–3670.
[11] Y. Xie, D.M. Cwiertny, Chlorinated solvent transformation by palladized zerovalent iron: mechanistic insights from reductant loading studies and solvent kinetic isotope effects, Environ. Sci. Technol. 47 (14) (2013) 7940–7948.
[12] Y.L. Han, C.J. Liu, J. Horita, W.L. Yan, Trichloroethene hydrodechlorination by Pd-Fe bimetallic nanoparticles: Solute-induced catalyst deactivation analyzed by carbon isotope fractionation, Appl. Catal. B Environ. 188 (2016) 77–86.
[13] G. Jiang, M. Lan, Z. Zhang, X. Lv, Z. Lou, X. Xu, F. Dong, S. Zhang, Identification of active hydrogen species on palladium nanoparticles for an enhanced electrocatalytic hydrodechlorination of 2,4-dichlorophenol in water, Environ. Sci. Technol. 51 (13) (2017) 7599–7605.
[14] D.M. Cwiertny, S.J. Bransfield, K.J.T. Livi, D.H. Fairbrother, A.L. Roberts, Exploring the influence of granular iron additives on 1,1,1-trichloroethane reduction, Environ. Sci. Technol. 40 (21) (2006) 6837–6843.
[15] J. Deng, E. Gao, F. Wu, Z. You, X. Li, S. Gao, L.-Z. Huang, Generation of atomic hydrogen by Ni-Fe hydroxides: mechanism and activity for hydrodechlorination of trichloroethylene, Water Res. 207 (2021), 117802.
[16] J. Alcántara, Ddl Fuente, B. Chico, J. Simancas, I. Díaz, M. Morcillo, Marine atmospheric corrosion of carbon steel: a review, Materials 10 (4) (2017) 406.
[17] J.D. Culpepper, S. Michelle?M, T.C. Robinson, N. Anke, C. David, D.E. Latta, Reduction of PCE and TCE by magnetite revisited, Environ. Sci.: Process. Impacts 20 (2018) 1340–1349.
[18] J. Deng, X. Zhan, F. Wu, S. Gao, L.-Z. Huang, Fast dechlorination of trichloroethylene by a bimetallic $Fe(OH)_2$/Ni composite, Sep. Purif. Technol. 278 (2022), 119597.
[19] L. Fang, R. Liu, L. Xu, J. Li, L.-Z. Huang, F. Li, Enhanced debromination of tetrabromobisphoenol a by zero-valent copper-nanoparticle-modified green rusts, Environ. Sci. Nano 6 (3) (2019) 970–980.
[20] L. Fang, L. Xu, J. Li, L.-Z. Huang, Copper nanoparticles/graphene modified green rusts for debromination of tetrabromobisphenol A: enhanced galvanic effect, electron transfer and adsorption, Sci. Total Environ. 683 (2019) 275–283.
[21] L. Fang, L. Xu, C. Liu, J. Li, L.-Z. Huang, Enhanced reactivity and mechanisms of copper nanoparticles modified green rust for p-nitrophenol reduction, Environ. Int. 129 (2019) 299–307.
[22] L.-Z. Huang, Z. Yin, N.G.A. Cooper, W. Yin, E.T. Bjerglund, B.W. Strobel, H.C. B. Hansen, Copper-mediated reductive dechlorination by green rust intercalated with dodecanoate, J. Hazard. Mater. 345 (2018) 18–26.
[23] S.T. Xiong, J.X. Zhao, B.L. Lun, F.M. Chen, Y.Y. Gong, F. Wu, J.H. Wu, L.-Z. Huang, W.Z. Yin, D.D. Dionysiou, Reconsidering the use of ferrous hydroxide for remediation of chlorinated ethylene contaminated groundwater: Ultra-fast trichloroethene dechlorination by ferrous hydroxide and bone char mixture, Chem. Eng. J. 438 (2022), 135516.
[24] J.X. Zhao, S.T. Xiong, F.M. Chen, W.Z. Yin, Y.Y. Gong, J.H. Wu, L.-Z. Huang, D. D. Dionysiou, One-time removal of Cr(VI) and carbon tetrachloride from groundwater by silicate stabilized green rust: The slow release of reactive sites driven by Fe(III)-Cr(III) oxides formation, Chem. Eng. J. 433 (2022), 134462.
[25] A.D. Becke, Density-functional thermochemistry. III. The role of exact exchange, J. Chem. Phys. 98 (7) (1998) 5648–5652.
[26] D.J. Van Hoomissen, S. Vyas, Early events in the reductive dehalogenation of linear perfluoroalkyl substances, Environ. Sci. Technol. Lett. 6 (6) (2019) 365–371.
[27] M.J. Frisch, G.W. Trucks, H.B. Schlegel, G.E. Scuseria, J.R.C.M.A. Robb, G. Scalmani, V. Barone, G.A. Petersson, H. Nakatsuji, X. Li, M. Caricato, A. Marenich, J. Bloino, B.G. Janesko, R. Gomperts, B. Mennucci, H.P. Hratchian, J. V. Ortiz, A.F. Izmaylov, J.L. Sonnenberg, D. Williams-Young, F. Ding, F. Lipparini, F. Egidi, J. Goings, B. Peng, A. Petrone, T. Henderson, D. Ranasinghe, V. G. Zakrzewski, J. Gao, N. Rega, G. Zheng, W. Liang, M. Hada, M. Ehara, K. Toyota, R. Fukuda, J. Hasegawa, M. Ishida, T. Nakajima, Y. Honda, O. Kitao, H. Nakai, T. Vreven, K. Throssell, J.A. Montgomery Jr., J.E. Peralta, F. Ogliaro, M. Bearpark, J.J. Heyd, E. Brothers, K.N. Kudin, V.N. Staroverov, T. Keith, R. Kobayashi, J. Normand, K. Raghavachari, A. Rendell, J.C. Burant, S.S. Iyengar, J. Tomasi, M. Cossi, J.M. Millam, M. Klene, C. Adamo, R. Cammi, J.W. Ochterski, R.L. Martin, K. Morokuma, O. Farkas, J.B. Foresman, D.J. Fox, GAUSSIAN 09, Gaussian, Inc., Wallingford, CT, 2009.
[28] J. Zhang, Q. Ji, H. Lan, G. Zhang, H. Liu, J. Qu, Synchronous reduction-oxidation process for efficient removal of trichloroacetic acid: H* initiates dechlorination and·OH is responsible for removal efficiency, Environ. Sci. Technol. 53 (24) (2019) 14586–14594.
[29] F. He, Z. Li, S. Shi, W. Xu, H. Sheng, Y. Gu, Y. Jiang, B. Xi, Dechlorination of excess trichloroethene by bimetallic and sulfidated nanoscale zero-valent iron, Environ. Sci. Technol. 52 (15) (2018) 8627–8637.
[30] Y. Luo, C. Zhou, Y. Bi, X. Long, B.E. Rittmann, Long-term continuous Co-reduction of 1,1,1-trichloroethane and trichloroethene over palladium nanoparticles spontaneously deposited on H_2-transfer membranes, Environ. Sci. Technol. 55 (3) (2021) 2057–2066.
[31] K. Yang, H. Peng, Y. Wen, N. Li, Re-examination of characteristic FTIR spectrum of secondary layer in bilayer oleic acid-coated Fe_3O_4 nanoparticles, Appl. Surf. Sci. 256 (10) (2010) 3093–3097.
[32] G. Liu, M. Feng, M. Tayyab, J. Gong, M. Zhang, M. Yang, K. Lin, Direct and efficient reduction of perfluorooctanoic acid using bimetallic catalyst supported on carbon, J. Hazard. Mater. 412 (2021), 125224.
[33] H.C. Bruun Hansen, C.B. Koch, Synthesis and characterization of pyroaurite, Appl. Clay Sci. 10 (1) (1995) 5–19.
[34] E. Kanezaki, S. Tanaka, K.-i Murai, T. Moriga, J. Motonaka, M. Katoh, I. Nakabayashi, Direct detection of a phase change in PdO/CeO_2 supported on χ-Al_2O_3 by means of in situ high-temperature measurements of XRD and FTIR, Anal. Sci. 20 (7) (2004) 1069–1073.
[35] Y. Liu, Q. Zhu, M. Tayyab, L. Zhou, J. Lei, J. Zhang, Single-atom Pt loaded zinc vacancies ZnO–ZnS induced type-V electron transport for efficiency photocatalytic H_2 evolution, Sol. RRL 5 (11) (2021) 2100536.

[36] K. Wiltschka, L. Neumann, M. Werheid, M. Bunge, R.A. During, K. Mackenzie, L. Bohm, Hydrodechlorination of hexachlorobenzene in a miniaturized nano-Pd(0) reaction system combined with the simultaneous extraction of all dechlorination products, Appl. Catal. B Environ. 275 (2020), 119100.
[37] D. Guerbois, G. Morin, G. Ona-Nguema, Nitrite reduction by biogenic hydroxycarbonate green rusts: evidence for hydroxy-nitrite green rust formation as an intermediate reaction product, Environ. Sci. Technol. 48 (8) (2014) 4505–4514.
[38] M. Tayyab, Y. Liu, S. Min, R. Muhammad Irfan, Q. Zhu, L. Zhou, J. Lei, J. Zhang, Simultaneous hydrogen production with the selective oxidation of benzyl alcohol to benzaldehyde by a noble-metal-free photocatalyst VC/CdS nanowires, Chin. J. Catal. 43 (4) (2022) 1165–1175.
[39] H. Zhang, D. Tian, J. Zhao, Structural evolution of medium-sized Pd(n) (n=15-25) clusters from density functional theory, J. Chem. Phys. 129 (11) (2008), 114302.
[40] G. Zanti, D. Peeters, DFT study of bimetallic palladium−gold clusters Pd_nAu_m of low nuclearities ($n + m \leq 14$), J. Phys. Chem. A 114 (2010) 10345–10356.
[41] S.H. Yuan, X.X. Liu, W.J. Liao, P. Zhang, X.M. Wang, M. Tong, Mechanisms of electron transfer from structrual Fe(II) in reduced nontronite to oxygen for production of hydroxyl radicals, Geochim. Et. Cosmochim. Acta 223 (2018) 422–436.
[42] L. Zhao, H. Dong, R.K. Kukkadapu, Q. Zeng, R.E. Edelmann, M. Pentrák, A. Agrawal, Biological redox cycling of iron in nontronite and its potential application in nitrate removal, Environ. Sci. Technol. 49 (9) (2015) 5493–5501.
[43] J.Z. Huang, A. Jones, T.D. Waite, Y.L. Chen, X.P. Huang, K.M. Rosso, A. Kappler, M. Mansor, P.G. Tratnyek, H.C. Zhang, Fe(II) redox chemistry in the environment, Chem. Rev. 121 (13) (2021) 8161–8233.
[44] K.A. Weber, L.A. Achenbach, J.D. Coates, Microorganisms pumping iron: anaerobic microbial iron oxidation and reduction, Nat. Rev. Microbiol. 4 (10) (2006) 752–764.